Collective headgroup conformational transition in twisted micellar superstructures

Francesca Baldelli Bombelli,[a] Debora Berti,*[a] Silvia Milani,[a] Marco Lagi,[a] Pierluigi Barbaro,[b] Göran Karlsson,[c] Astrid Brandt[d] and Piero Baglioni*[a]

Received 7th January 2008, Accepted 27th February 2008
First published as an Advance Article on the web 25th March 2008
DOI: 10.1039/b800210j

Predictions on amphiphilic self-assemblies traditionally rely on considerations on molecular shape and charge of the surfactant. In the case of functional surfactants a more sophisticated toolbox becomes necessary to design amphiphiles encoding chemical functionalities that provide additional responsive properties to their self-assemblies. Here we report on a comprehensive and combined structural–spectroscopic characterization of 1,2-dilauroyl-phosphatidyl-adenosine (DLPA) micelles in phosphate buffer. The temperature dependence, more precisely the thermal history of the sample, is explicitly taken into account. The experimental data, supplemented with MD simulations, indicate the presence of *two* possible states at room temperature, characterized by distinctly different structural properties that depend on the thermal history of the sample. The twisted superstructures, produced by aging DLPA micelles through intermicellar assembly of locally cylindrical aggregates at room temperature, collapse upon warming at 35 °C, yielding aligned filaments and/or wormlike structures. The initial superstructures cannot be recovered by thermal inversion. The reason for this behaviour is that the thermal activation causes a redistribution of *syn–anti* conformations of adenosine headgroups, as indicated by spectroscopic results (NMR, CD, FTIR), which is then collectively frozen thanks to molecular constraints present in the aggregate.

Introduction

Aggregation of amphiphilic molecules in well-defined supramolecular structures represents a convenient "bottom-up" route to soft nanostructured assemblies.[1–4] Amphiphilic building-blocks can spontaneously form aggregates with at least one length scale in the nanodomain, with a complex phase behaviour characterized by a large structural diversity, in terms of size, shape and interfacial flexibility of the assemblies. Geometric packing considerations on the molecular structure of the surfactants can give some clues in predicting the supramolecular structure of their aggregates.[2] These properties are ruled by thermodynamics, which provides control and reversibility of the equilibrium structural parameters mainly through variation of temperature and ionic strength. Variations at molecular level or of the solution conditions can alter the preferred spontaneous curvature of the surfactant film and induce strong changes at the mesoscopic scale.[3] Further, control parameters (*i.e.* photo-responsivity, redox activity, chirality, H-bonding ability) can be chemically encoded in the molecular precursors, as demonstrated by the recent developments in the field of functional surfactants.[5–11] As the molecular bricks become more and more sophisticated and additional control parameters are chemically introduced, it becomes central to assess how these added functionalities affect self-assembly and respond to variation of external conditions. Simple considerations on the relative sterical hindrances of the molecular portions (*i.e.* the packing parameter) are usually not sufficient, as polar heads do not merely interact through excluded volume and electrostatic repulsions. Among the recent advances in bio-inspired surfactants, some remarkable examples concern peptide–amphiphiles and nucleotide–amphiphiles.[8,9,12–14] The study of their structural and functional properties has also some important biological implications, since their chemical decoration, borrowed from naturally occurring molecules, can display selective interactions in bio-relevant processes and act as a template site for multiple-recognition-controlled fabrication of highly innovative nanomaterials.[15–19] In the last decade, we have studied self-assembly of phospholipids-based anionic nucleolipids,[20–25] PLN (phosphatidylnucleosides), where one single RNA nucleoside is enzymatically attached to the polar head of a lecithin substituting a choline headgroup.[26] Both the hydrophobic moiety and the nucleic headgroup have been varied to modulate the packing parameter and trigger/tune base–base interactions at the interface, in order to build-up different self-assemblies decorated by biological functionalities. Mixed PLN self-assemblies (micelles, bilayers, *etc.*) bearing complementary bases on the polar heads display interfacial interactions both through stacking and specific hydrogen bonds, according to a Watson–Crick pattern as in nucleic acids.[20,27]

The recent evidence of the binding of polynucleotides to small globular micelles formed by 1,2-dioctanoyl-phosphatidyl-adenosine[28] and of the sandwiching and ordering of polynucleotides in

[a]*Department of Chemistry and CSGI, University of Florence, Sesto Fiorentino, Florence, Italy. E-mail: berti@csgi.unifi.it; baglioni@csgi.unifi.it; Fax: +39 055 457 3036; Tel: +39 055 457 3033*
[b]*ICCOM CNR, Via Madonna del Piano, Sesto Fiorentino, Florence, Italy*
[c]*Department of Physical and Analytical Chemistry, Uppsala University, Sweden*
[d]*Hahn-Meitner Institute, Berlin, Germany*

between lamellar phases of 1-palmitoyl-2-oleoyl-phosphatidyl-adenosine[29] suggests that these nucleoamphiphiles can be exploited as compartmentalization and delivery systems for polynucleotides and oligonucleotides with relevance for many biomedical applications.

We have recently reported on the self-aggregation behaviour of DLPN focusing our attention on two complementary-pair derivatives, namely DLPA and 1,2-dilauroyl-phosphatidyl-uridine (DLPU), which have essentially the same packing parameter and molecular volume, but whose polar heads are characterized by different homo-stacking and H-bond constants.[23–25,30,31] These studies highlighted how self-assembly is strongly affected at the mesoscopic scale by molecular and chemical details of the amphiphile, not easily and merely ascribable to steric hindrance considerations. Freshly prepared solutions of both nucleolipids form wormlike micelles, as predictable from their packing parameter, but DLPA shows a concentration and time-dependent evolution to form twisted superstructures.[31] This different behaviour is due to stronger stacking interactions and H-bonds between adenine bases, inducing an intramolecular and intermolecular coordination that favours the formation of twisted aggregates.[31] The resulting self-assembled structure is thus determined by a delicate balance between headgroup interactions and surfactant-packing preferences.

The present study is motivated by the observation of an irreversible thermally-induced structural transition of DLPA twisted superstructures into cylindrical aggregates, which has sparked our interest in the molecular conformational details that drive such morphological change on the mesoscale.

Ganglioside micelles have also been found to exhibit different aggregates as a function of the thermal history of the sample:[32–34] their average aggregation numbers decrease upon heating and are not recovered if the sample is brought back to room temperature. This behaviour has been related to two different possible spatial arrangements of the bulky ganglioside headgroup in the aggregate: the temperature increase, in a confined medium as the micelle, drives a cooperative conformational transition between these two headgroup states that alter the packing preferences of the molecule in the aggregate and hence its size.

For interacting headgroups, a molecular conformational transition affects not only the packing parameter of the single molecule but, more importantly, the interaction pattern between the polar moieties, inducing a dramatic change in the micellar structure. The molecular design of novel functional surfactants clearly needs a deep understanding of the mechanisms of these conformational changes, how they can be triggered and how to assess their reversibility. In this scenario the conformational transition becomes a further control parameter of self-assembly behaviour.

This paper reports on the structural and spectroscopic characterization of DLPA self-assemblies as a function of their thermal history. A combination of Cryo-TEM (cryo transmission electron microscopy) with DLS (dynamic light scattering) and SANS (small angle neutron scattering) yields a structural characterization of DLPA micelles. These results are combined with CD (circular dichroism), NMR (nuclear magnetic resonance) and FTIR (fourier transform infrared spectroscopy) data, which provide information on the molecular scale. The aim of this combined investigation is to determine the molecular trigger that drives the mesoscopic transition.

Experimental

Materials

1,2-Dilauroyl-phosphatidyl-choline (DLPC) was purchased from Avanti Polar Lipids (Alabaster, Alabama, USA) and its purity checked by TLC. Uridine, HCl, $CHCl_3$, MeOH, and NH_3 (33% aqueous solution) used in the synthesis and NaH_2PO_4(>> 99%) and Na_2HPO_4 (>> 99%), were purchased from Fluka (Switzerland). Phospholipase D from *Streptomyces sp.* AA586 was obtained from Asahi Chemical Industry Co., Ltd (Tokyo, Japan). Deuterium oxide (>99.5%) for SANS measurements was purchased from Euriso-Top, (Saclay, Gif sur Yvette, France).

Synthesis of di-lauroyl-phosphatidyl-nucleosides

DLPA was synthesized starting from the corresponding phosphatidylcholine in a two-phase system according to a modification of the method proposed by Shuto and co-workers,[35] and obtained as an ammonium salt (Fig. 1A). The obtained product was purified through flash-chromatography and checked by NMR.

Sample preparation

DLPA samples were prepared by dissolving the lyophilized powder in 0.1 M phosphate buffer solution (PBS) at pH = 7.5. The aged samples were measured after 4 days at 25 °C, the annealed samples, after the aging treatment, were heated overnight at 35 °C. The annealed samples have been measured with DLS and CD for one week after the annealing, yielding time-invariant results.

The chemical analysis before and after annealing (NMR and TLC) has revealed no oxidation or lyso products for DLPA.

Methods

Cryo transmission electron microscopy (Cryo-TEM). The preparation of the samples for Cryo-TEM was performed[36] as

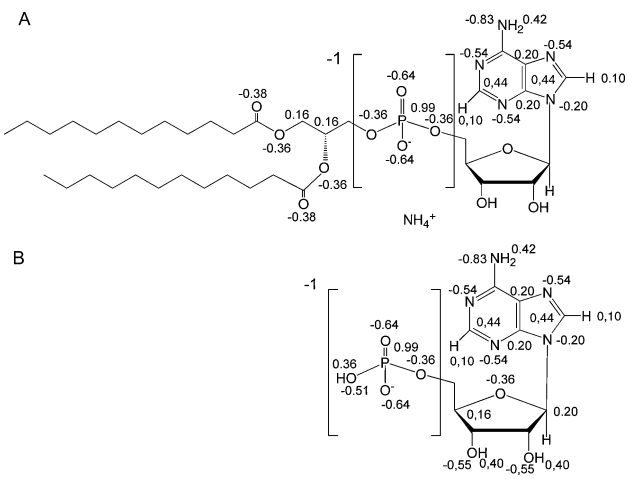

Fig. 1 Schematic drawings of the chemical structure of mono-anionic (A) DLPA and (B) AMP and of the partial charges in *e* units.

follows: within a climate chamber under controlled conditions with respect to temperature (25 °C) and relative humidity (98–99%), a small droplet of the solution was placed on a pre-treated 20 μm thick Cu grid, coated with a perforated cellulose acetate butyrate film. The excess material was removed by gently wiping off with a filter paper. The specimen was vitrified by a rapid transfer into liquid ethane close to its freezing temperature. The examination of the sample was then performed with a Zeiss 902A electron microscope operating in zero loss bright field mode at 80 kV. The temperature of the specimen was kept below −165 °C both during the transfer to the microscope and the examination. Digital images were recorded with a slow scan CCD camera (Proscan, Mooreweis, Germany) under focus settings of about 2–3 μm to enhance the image contrast.

Dynamic light scattering (DLS). Light scattering measurements were performed on a Brookhaven Instrument apparatus equipped with a BI9000AT correlator and a BI200SM goniometer. The signal was detected by an EMI 9863B/350 photomultiplier. The light source was the second harmonic of a diode pumped Coherent Innova Nd-YAG laser ($\lambda = 532$ nm), linearly polarized in the vertical direction. Approximately 0.5 ml of solution was transferred into the cylindrical Hellma scattering cell that was then sealed and centrifuged for about half an hour at 5000 g in order to remove dust particles from scattering volume.

In DLS experiments, the normalized time autocorrelation function $g_2(q,t)$ of the scattered intensity is measured according to:

$$g_2(q,t) = \frac{\langle I^*(q,0)\, I(q,t)\rangle}{\left\langle I(q,0)^2\right\rangle} \quad (1)$$

For ergodic systems, this function can be expressed in terms of the field autocorrelation function $g_1(q,t)$ through the Siegert relation:

$$g_2(q,t) = A[1 + \beta^2 g_1(q,t)^2] \quad (2)$$

where A is the baseline and β^2 is the coherence factor, dependent on the scattering geometry and details of the detection system. When the spectral profile of the scattered light can be described by a multi-Lorentzian curve, $g_1(q,t)$ can be written as the Laplace transform of the spectrum of relaxation times:

$$g_1(q,t) = \int_0^\infty w(\tau)\, e^{-\frac{t}{\tau}} d\tau \quad (3)$$

where τ is the relaxation time characteristic of the system, and $w(\tau)$ is its weight factor in the relaxation time distribution. In order to obtain a distribution $w(\tau)$ of decay rates, a constrained regularization method, CONTIN, developed by Provencher,[37] was used to invert the experimental data. A statistical parameter "probability to reject", P, is calculated for each $w(\tau)$ generated by CONTIN. The preferred solution is usually the one characterized by a P value closest to 0.5.

All the samples have been equilibrated for 1 hour at each investigated temperature, which is controlled with ± 0.1 °C accuracy.

Small angle neutron scattering (SANS). Small angle neutron scattering experiments were performed at the spectrometer V4 (BENSC-Hahn Meitner Institut-Berlin). Three different configurations (*i.e.* sample–detector distances: 1, 4 and 16 m) allowed to cover a range of wave vectors $q = (4\pi/\lambda)\sin(\theta/2) = 3.8 \times 10^{-3}$ Å^{-1} − 0.3 Å^{-1} with 6.1 Å neutrons and a wavelength spread $\Delta\lambda/\lambda \approx 10\%$. Deuterated phosphate buffer (0.1 M at pH = 7.5) was chosen as a solvent in order to enhance the scattering contrast and minimize the incoherent background from hydrogen. Data reduction has been accomplished according to standard BENSC[38] procedure for small angle isotropic scattering. All experiments were performed at a temperature of 25 °C ± 0.1 °C.

Circular dichroism (CD). Circular dichroism spectra were collected on a J-715 Jasco spectro-polarimeter. Hellma quartz cylindrical cells with variable path-length, selected not to exceed 0.8 optical density, were used. The observed circular dichroism was converted into molar ellipticity, normalizing for pathlength and dichroic chromophore concentration.

Nuclear magnetic resonance (NMR). ^{1}H NMR spectra were recorded on a Bruker Avance DRX-400 spectrometer operating at 400.13 MHz and equipped with a variable temperature control unit accurate to ±0.1 °C. Chemical shifts are relative to 5.0 × 10^{-2} M DSS solution in D_2O as external reference. Samples were prepared by dissolving the derivative in 0.50 ml of 0.1 M aqueous phosphate buffer (pH 7.5). The final lipid or nucleoside-monophosphate concentration was 2.0 × 10^{-2} M for each sample. The solutions were placed in an Evan's NMR tube, whose inner tube was filled with D_2O to provide a lock signal. Mono-dimensional ^{1}H NMR spectra were acquired using a Watergate sequence for the minimization of water signal.[39,40] Two-dimensional NMR spectra were recorded on non-spinning samples using pulse sequences suitable for phase-sensitive representations using TPPI. Each ^{1}H NOESY experiment was recorded twice using a Watergate water suppression sequence, 512 increments of size 2 K (32 scans each), mixing times of 12, 25, 50, 100, 200 ms and a relaxation delay of 1.5 s.[41,42] Each ^{1}H ROESY measurement was recorded twice using Watergate minimization, a low-power cw spin-lock pulse, 512 increments of size 2 K (with 16 scans each), 50 and 100 ms pulse for ROESY spin-lock and a relaxation delay of 1.5 s.[43,44]

Molecular dynamics (MD). We performed a set of simulations using the GROMACS v.3.3.1 package.[45,46] Both AMP (adenosine monophosphate) and DLPA molecules were modelled using the GROMOS96 force field parameter set 53A6,[47] which uses a united-atom representation for the aliphatic hydrocarbons, and therefore a simple point charge (SPC) water model. The partial atomic charges for AMP and DLPA in the simulations, chosen according to the literature for adenosine groups, are displayed in Fig. 1A–B.

Periodic boundary conditions (pbc) were applied: the border length of the simulation cubic cell was twice larger than the used finite-ranged potentials.

The interatomic potential, composed of a Lennard-Jones dispersion (LJ) and an electrostatic (ES) terms, used in the simulation is:

$$U(\mathbf{r}_{ij}) = \frac{q_i q_j}{4\pi\varepsilon_0 \mathbf{r}_{ij}} + 4\varepsilon_{ij}\left[\left(\frac{\sigma_{ij}}{\mathbf{r}_{ij}}\right)^{12} - \left(\frac{\sigma_{ij}}{\mathbf{r}_{ij}}\right)^{6}\right] \quad (4)$$

where i and j are the atomic species located at $\mathbf{r}_i$ and $\mathbf{r}_j$ respectively, $\mathbf{r}_{ij} = |\mathbf{r}_i - \mathbf{r}_j|$, q_i is the partial charge on atom i, ε_0 is the vacuum permittivity, while ε_{ij} and σ_{ij} are the standard LJ parameters for energy and size, respectively. The LJ interactions were truncated beyond the atom–atom cut-off distance of 1.4 nm, while the ES, calculated with the particle mesh Ewald method (PME),[48] at 0.9 nm. The integration of the Newton equations of motion was performed by using the Verlet leap-frog algorithm, and all the bonds were constrained using LINCS (linear constraint solver) algorithm.[49]

The simulations were performed in a NPT ensemble (isobaric-isothermal), where the temperature and the pressure were controlled by coupling the system with an external Nose-Hoover bath ($T_{initial}$ = 298 K, T coupling constant = 0.1 ps) and a Berendsen pressure bath (P = 1 bar, isothermal compressibility = $4.5.10^{-5}$ bar $^{-1}$, P coupling constant = 0.5 ps). Velocities were assigned according to the Boltzmann distribution at 298 K, and all coordinates and velocities were saved every ps. An energy minimization of 5000 steps with steepest descent algorithm was performed to stabilize the system and reduce the thermal noise. Finally, for all MD simulations the integration time step was 2 fs.

Dynamic simulations were performed on three different systems: 1) a single AMP molecule in 2163 SPC water molecules and 1 Na^+ ion (V_{box} = 64 nm^3) denoted as S1, 2) a single DLPA molecule in 4096 SPC water molecules and 1 Na^+ ion (V_{box} = 125 nm^3) denoted as S2, and 3) a total random configuration of 60 DLPA molecules, 60 Na^+ ions and 8654 water molecules (V_{box} = 330 nm^3, surfactant concentration $\sim$ 0.3 M) denoted as S3: all the simulations were 6 ns long. The water molecules that had their oxygen atoms closer than 2.7 Å from any nucleoside atom were removed. The initial ribose conformation is chosen C3′-endo and the φ dihedral angle set in *trans* (the atoms names and dihedral angle nomenclature are as in Saenger).[50]

Fourier transform infrared spectroscopy (FTIR). FTIR spectra were collected at room temperature with a Nexus 870 spectrophotometer (Thermo Nicolet, Paris), equipped with a pyroeletric detector (DTGS-TEC). The samples were measured in a 15 μm CaF_2 liquid cell, averaging 125 scans obtained with 4 cm^{-1} resolution. Data treatment was limited to solvent background subtraction. The achievement of a flat baseline around 2200 cm^{-1}, where only water combination modes are localized, was used as the confirmation of a correct background subtraction. FTIR spectra were recorded at room temperature on aged and annealed sample.

Results

Structural characterization

Cryo-TEM. We have previously shown that DLPA micelles exhibit time-dependent self-assembly to form twisted superstructures in a wide concentration range as illustrated in Cryo-TEM images A1–A3 reported in Fig. 2. A comparison with the behaviour of DLPU (U is a Watson–Crick partner of A in RNA and a weaker homo-stacker as compared to A), led to the conclusion that the complex self-aggregation behaviour of DLPA is driven by strong base-base interactions among adenosine headgroups

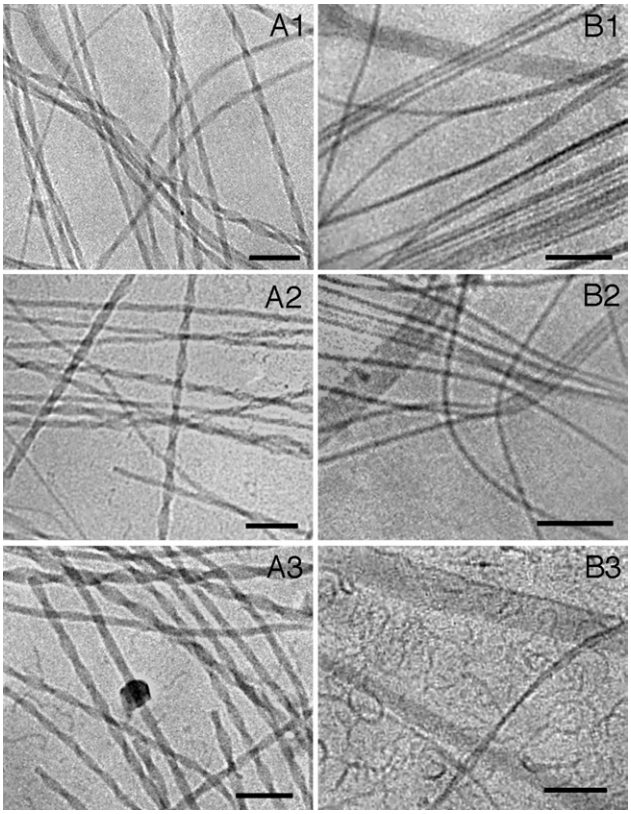

Fig. 2 Cryo-TEM images of DLPA micellar solutions in 0.1 M PBS. On the left, (1A–3A), aged samples at 25 °C 1 mM, 4 mM, 10 mM, respectively. On the right, (B1–B3), the same samples after an overnight annealing at 35 °C. The bar length is 100 nm.

at the micellar interface.[31] Moreover the formation of twisted superstructures occurs at the expenses of smaller wormlike micelles, whose global content averagely increases with surfactant concentration. This time-dependent self-aggregation takes place in a few days, after which the twisted structures are stable and no longer evolve from a structural point of view (aged samples). The present work is motivated by the observation that an overnight annealing at 35 °C of the aged DLPA samples (thereinafter annealed samples) causes a dramatic structural change of the aggregates that holds when the sample is brought back at room temperature. Hence, we have performed a Cryo-TEM investigation of the annealed DLPA samples as a function of the surfactant concentration. As it is shown in the micrographs B1–B3 in Fig. 2 (DLPA 1 mM, 4 mM, 10 mM, respectively), the input in thermal energy induces the unwinding of the twisted superstructures for all DLPA concentrations investigated. Since the winding of micellar threads to form twisted structures was attributed to stacking directional interactions, it is reasonable to assume that it is a strong destacking process that promotes this breaking-off. A surfactant concentration trend can be observed in the annealed samples: for the lower DLPA concentrations (Fig. 2, B1–B2) they are mostly composed by giant elongated micelles of diameter about 7 nm (from now on called filaments) whose local structure seems cylindrical, while in the most concentrated sample the wormlike phase is dominant (Fig. 2, B3). The filaments, in some cases, are strongly aligned along their contour lengths in a sort of large strip. These

elongated structures were also observed in some of the fresh DLPA samples and identified as the structural units of the twisted superstructures,[31] strengthening the hypothesis that they originate from their dissociation.

Dynamic light scattering. DLS experiments of aged 4 mM DLPA micellar solution have been performed as a function of temperature at a scattering angle $\theta = 90°$. The auto-correlation functions are reported in Fig. 3A as a function of a reduced time unit, t^*, that takes into account the variation of the solution viscosity and refractive index induced by the temperature change in the following way:

$$t^*(T) = t\left[\frac{T}{T_{25}}\frac{\eta_{25}}{\eta}\frac{n^2}{n_{25}{}^2}\right] \quad (5)$$

where T_{25}, η_{25}, n_{25}, T, η, and n are the temperature (expressed in K), the viscosity of the medium and the refractive index at 25 °C (taken as a reference) and at temperature T, respectively.

These parameters appear in the diffusion coefficient (T, η) and in the scattering vector (n) thus affecting the experimental relaxation time. With this normalization of the independent variable, any differences seen in the autocorrelation functions are directly correlated to T-induced structural changes.

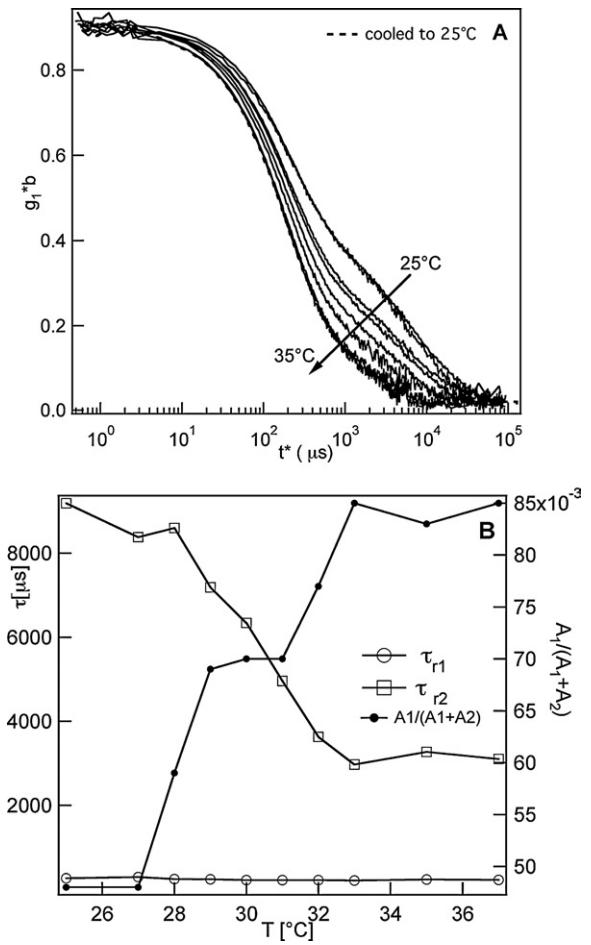

Fig. 3 (A) DLS autocorrelation functions for aged 4 mM DLPA micellar solutions in 0.1 M PBS at pH = 7.5 as a function of temperature (25–35 °C) at a scattering angle $\theta = 90$. (B) Relaxation times, τ_{r1} (○) and τ_{r2} (□), inferred from CONTIN analysis of the autocorrelation functions reported in part A, as a function of temperature. On the right hand y-axis it the relative abundance of τ_{r1} population is also reported.

Two components are clearly distinguishable in the auto-correlation functions. When T is raised, the slowest relaxation component decreases, although it never vanishes. A Laplace inversion of the auto-correlation functions, performed with the algorithm CONTIN,[37] yields, for each temperature, two populations well-resolved on the relaxation time axis. A plot of these relaxation times as a function of the temperature, reported in Fig. 3B, shows that a decrease of the slowest relaxation is triggered at 28 °C until a plateau value is approached above 33 °C.

The slowest relaxation time is related to the diffusion of superstructures (twisted structures or filaments) larger than the wormlike micelles: presumably the diffusion of the twisted aggregates is slower than the filaments, so the decrease of the slowest component (both in relaxation time and amplitude) is explained with the breakdown of the twisted superstructures. Furthermore, the fastest relaxation time, correlated to the wormlike micelles diffusion,[31] remains more or less constant with temperature, but its amplitude (see Fig. 3B) increases considerably until 33 °C, indicating that the collapse of the twisted micelles leads to the formation of both filaments and wormlike micelles.

An important observation is that the autocorrelation function of annealed DLPA micellar solution at 25 °C (dotted line in Fig. 3A) is the same as at 35 °C, and it is time-invariant, indicating that a further self-aggregation is prevented and no reversibility occurs.

Small angle neutron scattering. SANS experiments have been performed on aged DLPA micellar solutions in PBS 0.1 M (pH = 7.5) at 25 °C before and after annealing treatment.

Fig. 4A and C show SANS spectra of 5 mM and 10 mM aged and annealed DLPA micellar solutions, respectively. The logarithmic plots highlight in the intermediate–low q-region a $q^{-\alpha}$ scaling behaviour, with α higher than 1 for the aged samples. The scaling exponent approaches 1 (the signature of locally cylindrical micelles) as DLPA concentration increases, passing from 1.4 to 1.2.

Cryo-TEM images show the simultaneous presence of different morphologies of aggregates in the same aged samples (Fig. 2 A1–A3), *i.e.* twisted superstructures, elongated filaments and a wormlike phase. Therefore, it is reasonable to ascribe this unusual low q-dependence to the superposition of coexisting different scaling behaviours, rather than to a single characteristic aggregate dimensionality or shape. The deviation from the scattering law for cylindrical shapes is less important for the most concentrated sample, where the wormlike content is higher, as Cryo-TEM micrographs show (Fig. 2). It is worthwhile to remember that for DLPU in this concentration range the scattering law for locally cylindrical aggregates clearly emerges and persists irrespectively of the aging and of the thermal history of the sample.[23,25]

Let us consider the effect of warming: upon annealing these spectra show a general decrease of the forward scattering intensity, while differences are weak at higher q-values.

This decrease is accompanied by a decrease of the exponent of the scattering power law, which distinctly approaches 1, as shown by the dotted lines in Fig. 4A and C.[51] This feature is

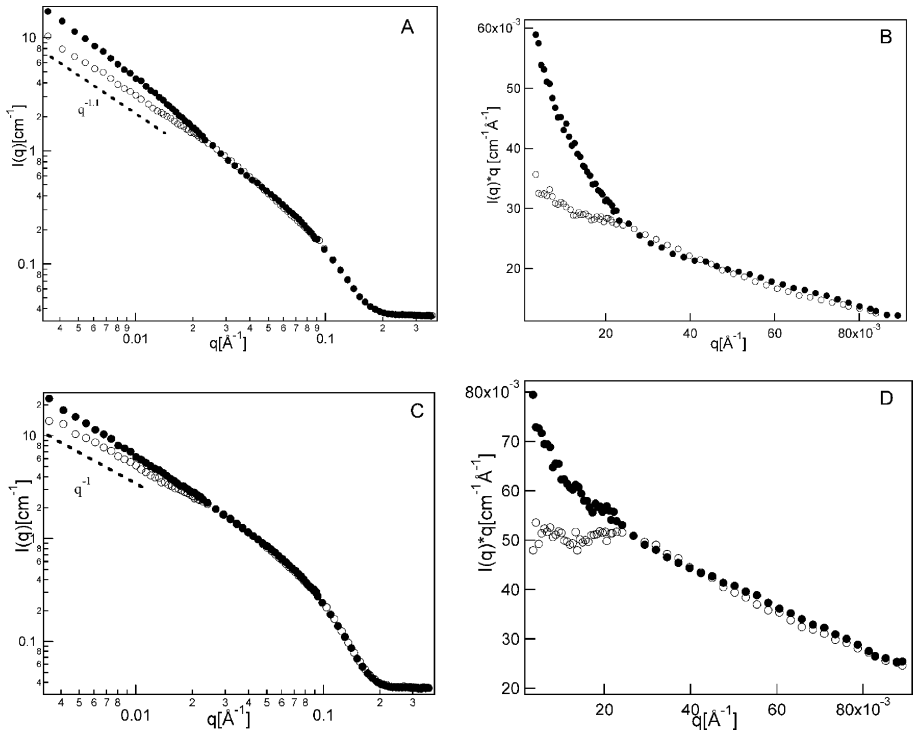

Fig. 4 A, C) SANS spectra of aged and annealed DLPA micellar solutions in PBS 0.1 M pH = 7.5 at different DLPA concentrations, 5 mM and 10 mM, respectively. B, D) Holtzer or bending-rod plots of DLPA SANS spectra reported respectively in A) and C) pictures. This representation of SANS spectra emphasizes the region with scaling power −1 as a plateau, it appears evident that this region is not present in the spectra at 25 °C for both DLPA concentrations. (●) Aged samples at 25 °C, (○) annealed samples measured at 25 °C.

better highlighted in the Holtzer or bending-rigidity plots,[52] reported in Fig. 4B and D. The q^{-1}-region appears as a plateau for both annealed samples while it is clearly not present for the samples aged at 25 °C.

The behaviour is however still very different from what is observed for a pure DLPU wormlike phase, as shown in Fig. 5A–B,[23,25,30] reporting the Holtzer plots of DLPU micellar solutions compared with the spectra of annealed DLPA at the same concentrations. For the most dilute DLPA sample (Fig. 5A), this Holtzer representation highlights a remarkable scaling difference, meaning that the wormlike phase is not dominant and the filaments provide a large contribution, in agreement with Cryo-TEM results. For the 10 mM sample (Fig. 5B), the two spectra are very similar except for the lack of the low-q upturn connected to different flexibility of DLPA and DLPU micellar structures.

Spectroscopy

Circular dichroism. CD can provide information on headgroup–headgroup interactions, allowing a correlation between the electronic properties of the nucleic bases and the overall structure of the aggregate, as determined through scattering techniques. The electronic structure of nucleic bases has been extensively reported in the classical literature.[53–56] The chromophores themselves do not display an intrinsic CD since they have a plane of symmetry; the low-intensity signal shown by nucleotides and nucleosides derives from the interactions of the base with the asymmetric sugar. Macromolecular organization in nucleic acids and polynucleotides, driven by base–base interactions, induces a so-called super-asymmetry that enhances CD bands. CD is, therefore, a valuable method to monitor the conformation of both nucleic acids and polynucleotides and their changes in response to external stress.[57–60]

We previously reported a CD investigation on DLPA micellar solutions as a function of time and concentration.[31] The formation of twisted superstructures causes a remarkable positive Cotton effect at about 260 nm, indicating a strong stacking excess and also a predominance of anti conformation (positive signal, as can be seen in Fig. 6A–C, empty squares) for the adenine bases at the micellar interface.[61,62]

It is known that nucleotides can adopt two main orientation of the base with respect to the glycosidic bond (Fig. 7), namely *syn* and *anti*, defined in terms of the glycosidic torsion angle, χ, (O4′–C1′–N9–C4 for purines and O4′–C1′–N1–C2 for pyrimidines): the *syn* conformations correspond to $\chi = 0° \pm 90$ and the *anti* conformations correspond to $\chi = 180° \pm 90$.[50,63]

Several NMR and CD spectroscopic data in the literature[64–70] report that nucleosides and nucleotides in solution display a rapid *syn*↔*anti* interchange equilibrium. Regarding the population of the two conformational states, the *anti* conformation is predominant for most nucleosides, while the *syn* population is higher for purines. The orientation adopted by the base is largely affected by the furanose puckering, that can be described as C2′-*endo* or C3′-*endo*.[71–74] It has been also reported that for ribonucleotides, purines (*i.e.* adenosine) prefer the C2′-*endo* (S type) and pyrimidines (*i.e.* uridine) the C3′-*endo* (N type), while for deoxyribonucleotides both bases are preferentially in

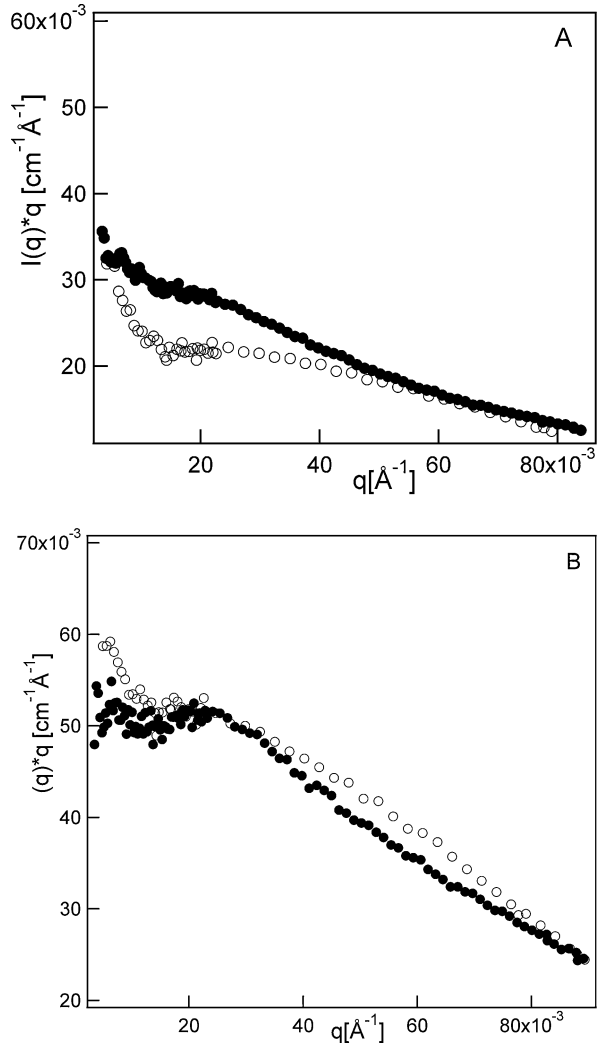

Fig. 5 Holtzer or bending-rod plots of DLPU and annealed DLPA micellar solutions at 25 °C at the same surfactant concentration. DLPU forms a pure wormlike micellar phase in this concentration regime. A) 5 mM B) 10 mM. (●) DLPA (○) DLPU.

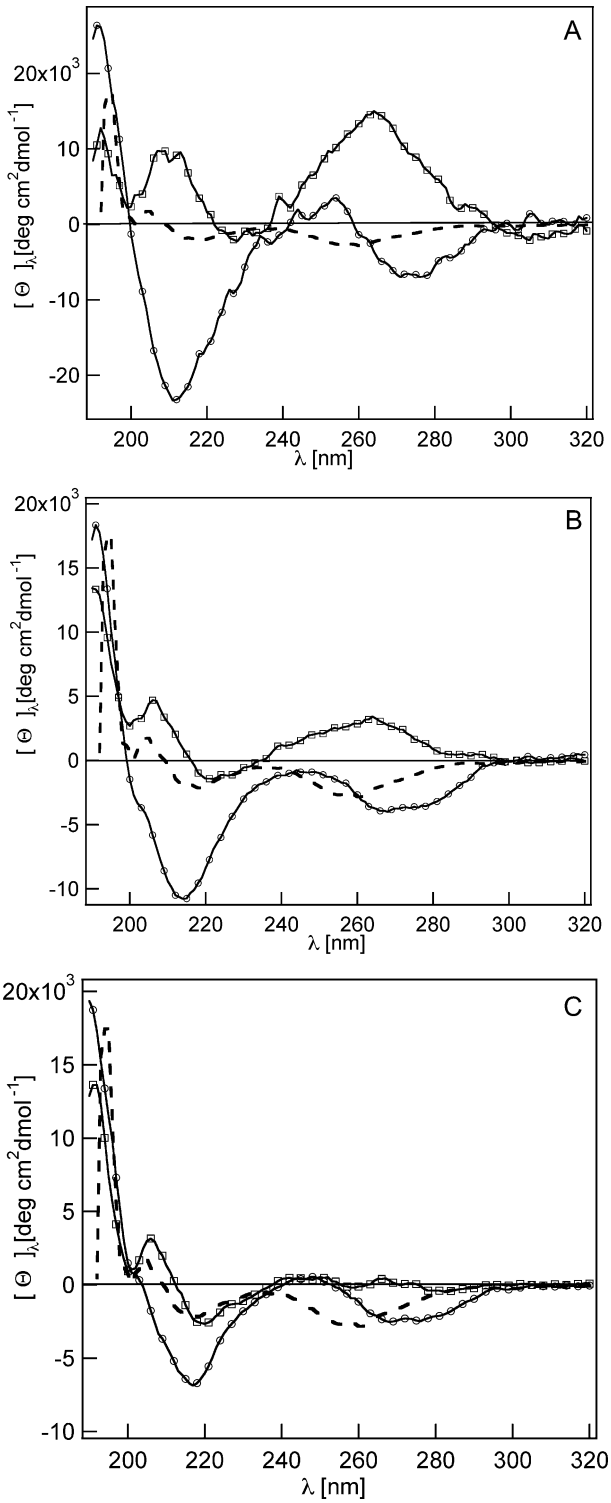

Fig. 6 A–C) CD spectra of aged and annealed DLPA micellar solutions in PBS 0.1 M at pH = 7.5, respectively for DLPA 1, 4 and 10 mM. (□) aged sample, (○) annealed sample, (dotted line) r-AMP at the same DLPA concentration.

the C2′-*endo* (S type).[64] Furthermore, for rA and rU the *syn* orientation is usually associated with the C2′-*endo* ribose conformation and the *anti* with the C3′-*endo* (see Fig. 8).

The comparison of DLPA spectra to that displayed by single nucleotides in solution (dotted line in Fig. 6A–C, for which the *syn* configuration is favoured), indicates that DLPA self-assembly into twisted superstructures, shifts the *anti–syn* equilibrium towards *anti*. This effect is concentration-dependent: as the volume fraction is increased, the energy associated with the *anti* conformation is more and more similar to the *syn* one in the aggregate, until they eventually become equivalent (Fig. 6C, empty square).

However, the most noteworthy feature of these spectra is the effect of thermal annealing of the aged sample: the Cotton effect is reversed, meaning a significant change in the base environment. Fig. 6A–C shows this behaviour for different concentrations.

A temperature scan of CD spectra for 1 mM DLPA micellar solution (Fig. 9) illustrates a continuous decrease of the positive signal at 260 nm, together with the increase of the negative peaks centred at 285 and 210 nm, with the temperature until the sign reversal above 32 °C. At this temperature the positive Cotton effect vanishes and the whole spectral shape changes completely. If the sample is then brought back to room temperature, the

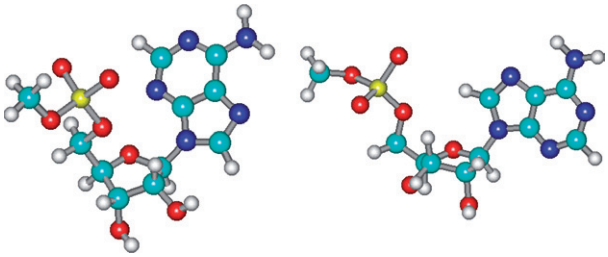

Fig. 7 Geometrical optimization of the molecular structure of methyl-AMP: comparison between *syn* and *anti* adenosine conformations. (Left) *anti* conformation; (right) *syn* conformation.

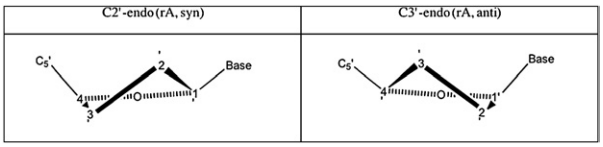

Fig. 8 Schematic drawing of the more common ribose puckering conformations in nucleic acids: C2′-*endo* (south conformation, S) and C3′-*endo* (north conformation, N).[50,63]

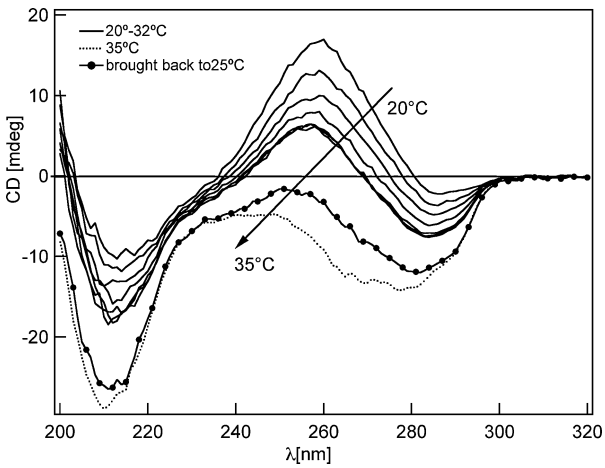

Fig. 9 CD spectra of 1 mM aged DLPA micellar solution as a function of the temperature.

original spectral shape is no longer recovered. The CD sign inversion indicates a significant change in the base environment that cannot be only due to an unstacking effect (there is no significant decrease in intensity), but can be caused by a conformational transition of the nucleoside. The CD signal of the annealed samples is, in fact, very similar in the shape, two negative bands at 260–280 nm and 210–220 nm, respectively, to the CD signal of r-AMP in solution where it is known that *syn* population is larger. This could indicate a shift of the *syn*⇆*anti* equilibrium towards the *syn* conformer. This form is then "frozen" on the micellar surface and, upon returning to room temperature, the conversion to the anti form is not allowed.

^{1}H-2D nuclear magnetic resonance. Nuclear cross-relaxation is one of the most informative sources for the determination of molecular structure in solution.[75] Particularly, the nuclear Overhauser effect measured by two-dimensional NOE spectroscopy (NOESY) or rotating frame Overhauser effect spectroscopy (ROESY) has become indispensable for the analysis of time-averaged molecular conformation of biological molecules since it is able to provide an estimate of the inter-proton distances by the accurate determination of the ^{1}H NOE cross-peaks intensities.[76] The internuclear distances are related to these intensities by the inverse sixth power r^{-6}.[77] In order to investigate the temperature dependence of the relative populations of *syn*/*anti* conformers headgroups in DLPA micelles, we recorded both ^{1}H NOESY and ^{1}H ROESY experiments on aged 20 mM DLPA micellar solutions in the range 15–35 °C, using mixing (spin-lock) times ranging from 12 to 200 ms.[78] The choice of these latter values is motivated by the need to minimize spin-diffusion effects.[79] Conformational analysis was carried out taking into account the H_8–H_1' and H_2–H_1' protons distances that are different in the two conformations, since significant overlapping of the other ribose resonances, mostly due to ^{1}H NMR signals broadening in the micellar solutions, prevented us from an accurate measurement of their individual cross-peaks. Despite the complexity of the macromolecular system investigated, which is well away from being conformational rigid and for which the isolated proton couple approximation may not hold,[80] preventing a quantitative determination of inter-proton distances, a qualitative estimate of the changes in the relative H_8–H_1' and H_2–H_1' distances upon temperature variations can be obtained from the ratio of the corresponding NOE cross-peaks intensities. Intensities were measured from cross-peaks volume integration. The same approach was previously adopted in order to evaluate the ratios of internuclear distances in lithium alkenyls.[81]

The analysis of 2D NMR data obtained shows that under our experimental conditions the micellar system falls in the *slow tumbling* motional regime ($\tau_c \gg 1/\tau_L$) as only negative (positive phased) NOEs are observed (see Fig. 10 as example).[74c]

More importantly: 1) well-resolved, intramolecular H_8–H_1' and H_2–H_1' NOE cross-peaks are detected in all the experiments recorded; 2) irrespective of the temperature, the H_8–H_1'/H_2–H_1' cross-peaks intensities ratio is always greater that 1 (see Fig. 10); 3) irrespective of the mixing time, the H_8–H_1'/H_2–H_1' cross-peaks intensities *ratio increases on increasing the temperature* (Fig. 11).

The above findings indicate that the H_2, H_8 and H_1' protons can be safely used as significant reporters for the conformation of nucleoside polar heads in DLPA micelles, through the evaluation of their 2D NOE cross-peaks intensities. Particularly, we can conclude that: 1) compared to the H_2–H_1' proton distance, the H_8–H_1' elongation is always significantly shorter under our experimental conditions, *i.e.* in the temperature range 15–35 °C (this is in line with the results from MD simulations, *vide infra* Table 1); 2) compared to the H_2–H_1' distance, the H_8–H_1' distance *unequivocally decreases on increasing the temperature*. This result clearly shows that *the base orientation with respect to the sugar changes on increasing the temperature*. Analogous conclusions can be obtained from the examination of ^{1}H ROESY spectra.

Molecular dynamics. The NMR results demonstrate that a temperature increase induces a structural change at the

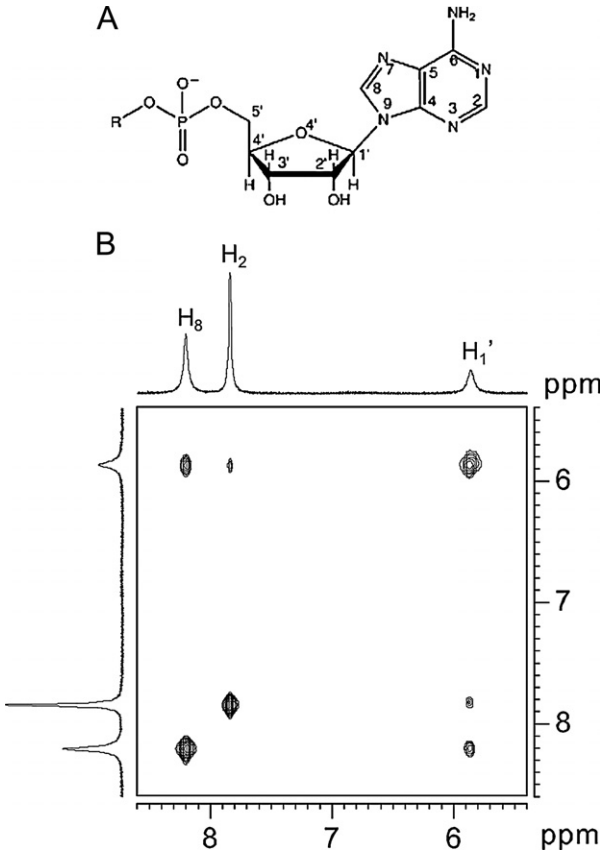

Fig. 10 A) Structure of Adenosine monophosphate showing the conventional atom numbers. B) Section of the ^{1}H NOESY spectrum of 20 mM DLPA (0.1 M PBS, pH 7.5, 15 °C, τ_m 50 ms).

molecular level in the nucleoside conformation. However, an estimate of the interatomic distances between DLPA nucleoside protons in the two conformations, *syn* and *anti*, is required to know which one is favoured upon heating and to explain the

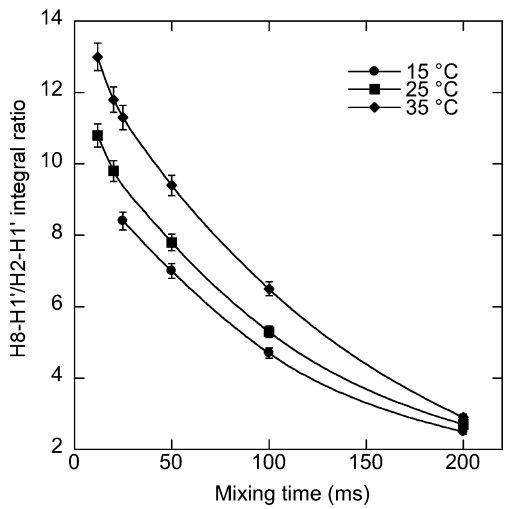

Fig. 11 Plot of the H_8–H_1'/H_2–H_1' cross-peaks intensities ratio as a function of the mixing time (from 20 mM DLPA ^{1}H NOESY spectra in 0.1 M PBS, pH 7.5). Data recorded at: (◇) 15 °C, (□) 25 °C and (△) 35 °C.

Table 1 Interatomic distances between H_8 and H_2 (base) and H_1' and H_2' (sugar) for the most common adenosine conformations inferred considering the most populated dihedral angles of the distributions from the MD simulations of the system S3 (χ_{anti} max = 218°, χ_{syn} max = 50°)

	C2′*endo* *anti*/Å	C2′*endo* *syn*/Å	C3′*endo* *anti*/Å	C3′*endo* *syn*/Å
H_8–H_1'	3.9	2.6	3.9	2.7
H_2–H_1'	4.4	6.0	4.4	6.0
H_8–H_2'	3.8	4.4	2.5	2.5
H_2–H_2'	5.9	5.0	4.5	4.5

experimental results. A more quantitative evaluation of the interatomic distances between adenosine hydrogen atoms of DLPA molecules arranged in cylindrical micelles can be obtained from MD simulations (System S3, see methods), whose results reported in Fig. 12. Starting from a completely random spatial distribution (Fig. 12A), DLPA molecules self-assemble in the first 4 ns of simulation as a cylindrical micelle that covers with uniform cross-section the whole box length (Fig. 12B–C, cross-section and side views, respectively). Moreover, the periodic boundary conditions allow particles on one border to interact with the image of the molecules at the other border of the cell, making the simulated structure a real cylindrical micelle, notwithstanding the finite length (7 nm) of the box. This MD result, *i.e.* the preference towards locally cylindrical packing, is in full agreement with experimental results from scattering and Cryo-TEM techniques.

The distances between H_8 and H_2 (base) and H_1' and H_2' (sugar) were inferred considering the most populated dihedral angles of the distributions from DLPA simulated micelles (χ_{anti} max = 218°, χ_{syn} max = 50°) and are reported in Table 1. On the basis of these findings the fact that the distance H_8–H_1' decreases and/or H_2–H_1' increases if T is increased, as observed in 2D NMR experiments, can be explained by an increase of the overall *syn* population of the nucleoside polar heads arranged in micelles.

MD simulations can also be exploited to have information on molecular structural parameters of the nucleoside moieties on

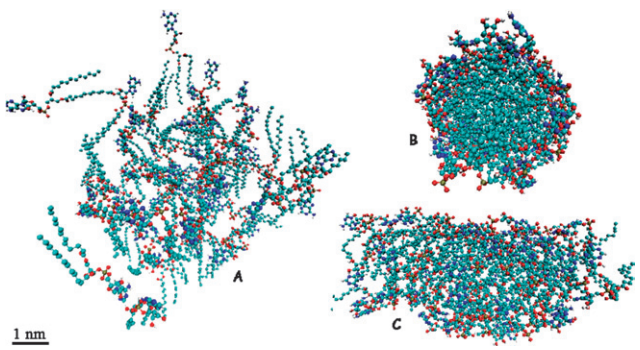

Fig. 12 Snapshots visualized through VMD[87] renderings of the simulation for S3 system (water and sodium molecules are hidden for clarity): A) initial random configuration of 60 DLPA molecules, B) front view of the micelle cross-section C) lateral view of the rod-like micelle. B) and C) snapshots are after 6 ns. Lipid hydrocarbon tails appear in green, N atoms in blue, P in brown and O in red.

the micellar surface. Unfortunately, DLPA *syn–anti* transition in the micellar state is not accessible to our MD simulation: its correlation time (6 ns for a free adenosine in solution) is too long to infer any meaningful statistics of this process.[82] Longer simulations would be needed to characterize this conformational space. On the other hand, we can get information from MD results about the sugar puckering (as we have seen in riboucleotides a C2′-*endo* puckering is generally correlated with the *syn* conformation)[64] whose motions have a reasonable time scale to be studied *via* molecular dynamics also for nucleic acids in solution.[83,84] The evaluation of the puckering distributions was performed by calculating the probability of the sugar puckering distribution in C3′-*endo* and C2′-*endo* by means of the parameter *P*, the pseudorotation angle, that was determined according to RWS formulation (Rao, Westhol and Sundraligam).[85] In order to evaluate the quality of our simulation concerning the sugar puckering, we also ran the simulation for r-AMP in solution (system 1 in methods) for which we found a probability of the C2′-*endo* conformation of about 70%, which is in good agreement with both previous experimental[86] and theoretical findings.[82]

Without entering into the details of r-AMP simulation, the good agreement of the structural parameters extracted from MD calculations with those reported in the literature validates the force field used for this system. If we extend our analysis to a single DLPA molecule in solution (S2 system in methods), the addition of the glycerol backbone with two C12 aliphatic chains (Fig. 2) induces an enhancement of the preference for the C2′-*endo* puckering that is even more accentuated for micellar DLPA system. The increase of the C2′-*endo* population can be due to a decrease of hydration passing from the monomers to the micelles, as it is known that ribose–water interactions affect the sugar conformations,[82] (particularly stabilizing the C3′-*endo* configuration through H-bonds with O3′H3′ and O2′H2′). In fact, the average number of H-bonds for molecule with the solvent, calculated from the simulations, decreases in this trend: r-AMP (3.2) > DLPA-monomer (2.8) > DLPA-micelle (2.1). The high preference for C2′-*endo* puckering (more often associated with *syn* conformation) can favour the transition from *anti* to *syn* in adenosine headgroup on DLPA micelles upon thermal treatment.

Fourier transform infrared spectroscopy. It is known that different base–sugar conformations both in nucleotides and in nucleic acids are responsible for marker bands in the infrared spectrum, mainly in the 1400–1250 cm^{-1} region.[50,88] For purines in *anti* conformation these marker bands are displayed in the range 1380–1370 cm^{-1}, while a *syn* conformation causes a shift to 1357–1352 cm^{-1}.[89–91]

However, other absorption contributions due to the lipid tails, namely CH_2-wagging and CH_3-scissoring, are present in this spectral region for DLPA.[92–94] Since the bending vibration modes of the tails are not affected by the base conformation and FTIR spectra of aged and annealed samples were performed at the same temperature, 25 °C, the wagging vibrations can be safely regarded as independent of the thermal history of the sample. Any variations in this spectral region can thus be associated to a change of the *syn–anti* conformation equilibrium.

Fig. 13 compares the FTIR spectra of 35 mM aged and annealed DLPA micellar solutions. The peak centred at

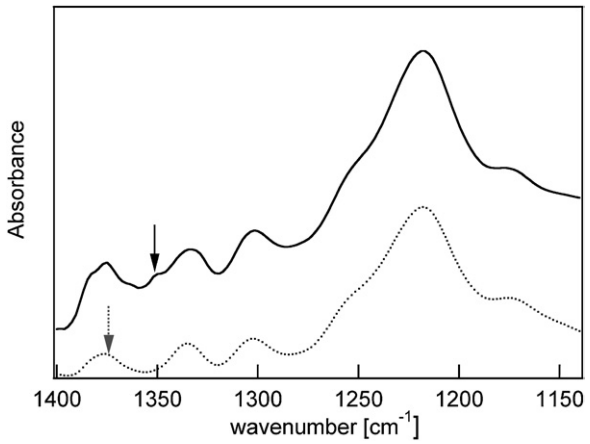

Fig. 13 FTIR absorption spectra of DLPA 3.5×10^{-2} M micellar solution in PBS 0.1 M at pH = 7.5 at 25 °C: (dotted line) aged sample and (solid line) annealed sample. The arrows indicate the marker bands for *anti* (dotted) and *syn* (solid) conformations.

1375 cm^{-1} for the aged sample indicates that the *anti* conformation seems to be predominant. The thermal treatment causes the appearance of a pronounced shoulder at approximately 1350 cm^{-1}, that confirms the presence of DLPA molecules in the *syn* conformational state.

Discussion

Cryo-TEM, DLS and SANS experiments on DLPA micellar solutions in PBS, performed as a function of the temperature and the thermal history of the sample, provide evidence that DLPA aggregates undergo a structural transition upon thermal treatment, consisting of an overnight annealing at 35 °C.

More specifically, Cryo-TEM images clearly illustrate that a thermal activation drives the breakdown of twisted superstructures occurring in DLPA annealed samples, yielding both filaments and wormlike micelles. A DLS study shows the presence of two populations of relaxation modes in the whole temperature range investigated, indicating the presence of different kinds of aggregates. If compared with Cryo-TEM observation, DLS allows us to relate the slower relaxation time to the larger superstructure diffusion, whose collapse can be continuously monitored as *T* is increased as a decrease both of relaxation time (smaller aggregates) and of its relative amplitude with respect to the overall aggregate populations. SANS spectra are in agreement with this scenario and indicate moreover a clear concentration-dependence, causing the wormlike phase to be the dominant one at the highest DLPA concentration, as also shown by the Cryo-TEM images.

The picture that emerges from the combined structural observation in direct and reciprocal space, is that DLPA micelles, upon thermal activation slightly above room temperature, undergo a structural transition, which cannot be reverted upon *T* decrease; therefore, beside classical considerations based on thermal equilibrium (affected by *T*, surfactant volume fraction, medium ionic strength), predictions about structural properties must take into account the thermal history of the sample. Moreover, a more effective approach, which can help molecular design of functional surfactants, mandatory requires the investigation

to be shifted on the molecular scale. Since DLPU micelles do not display such a complex behaviour, and thermal treatments are completely reversible, the explanation must reside in the peculiarity of the polar head.

CD, FTIR and NMR (supplemented by MD simulations) data on aged and annealed DLPA micellar solutions concur to demonstrate that this structural transition at the mesoscale is driven by redistribution of DLPA molecules populating the *syn* and *anti* conformational states of the adenosine headgroups. The thermal input produces a shift in the *syn–anti* equilibrium toward the *syn* orientation. While the *anti* conformation seems to be the dominant one in the twisted superstructures at RT, the *syn* form is more and more populated as the temperature is raised. This molecular transition dramatically alters DLPA super self-assemblies morphology, in a "frozen" collective conformation, which cannot be reverted back once room temperature is recovered.

It is known that the molecular shape of chiral surfactants sets the preferred tilt angle between neighbouring molecules in the aggregate significantly influencing its structure, mostly for tubules, twisted and helical micelles.[95–97] The drastic concentration dependence of the CD signal indicates in this case that a molecular conformational change at the headgroup level not only alters the surfactant structure, but also, modifies the interaction pattern of adenine bases on the aggregate surface. Hence, a balance between headgroups interactions and surfactant-packing interactions determines the resulting self-assemblies.

It is noteworthy to remind the reader that whilst nucleotides in solution undergo a rapid *syn–anti* interchange,[50] in this system, within a micellar surface, *i.e.* a geometrical constrained space with respect to a bulk medium, the rotational freedom of the base is severely hindered. Hence, producing a shift of the *anti–syn* base conformational equilibrium towards the *syn* one on the micellar surface, where each base strongly interacts with the neighbouring ones, becomes part of a collective rearrangement that impacts the mesoscopic scale as a dramatic structural transition of the aggregates.

Conclusions

This paper combines structural observation in direct and reciprocal space and spectroscopic investigation of DLPA micellar solutions, as a function of surfactant volume fraction, temperature and thermal history of the sample. A combination of DLS, SANS and Cryo-TEM provide evidence that two states, characterized by markedly different structural properties (namely presence of intermicellar twisted superaggregates, local nature of the self-assemblies, preferred local curvature), can be observed at room temperature, depending on the thermal history of the sample.

The main conclusions of this work, gathered from a combination of complementary spectroscopic techniques, is that the molecular explanation for this mesoscopic behaviour is that in DLPA micelles even a transient temperature increase irreversibly displaces the *syn–anti* conformer equilibrium towards the *syn* form. This transition occurs in a collective fashion at the micellar surface and causes irreversibly a structural change of the aggregates. The understanding of the molecular mechanism that drives the structural transition at the mesoscale is of fundamental importance in the perspective to exploit these lipids as template for material scaffolding in nanotechnology. This can significantly help in the design of the molecular structure of functional surfactants in order to obtain the desired self-assembled structure at the mesoscale.

Acknowledgements

The authors wish to thank CSGI and MIUR (PRIN-2006) for funding the research. This research project has been also supported by the European Commission under the 6th Framework Programme through the Key Action: Strengthening the European Research Area, Research Infrastructures. Contract no. RII3-CT-2003-505925 (NMI3). F.B.B. acknowledges financial support from the European Commission's 6th Framework Programme (Project reference AMNA, Contract no. 013575).

References

1 S. A. Safran, *Thermodynamics of Surfaces, Interfaces, and Membranes*, Addison–Wesley, New York, 1994.
2 J. N. Israelachvili, *Intermolecular and Surface Forces*, Academic Press, San Diego, 2nd edn, 1992.
3 J. H. Fuhrhop and J. Koning, *Membrane and molecular assemblies: the synkinetic approach*, The Royal Society of Chemistry, London, 1994.
4 J. M. Lehn, *Supramolecular Chemistry: Concepts and Perspectives*, Wiley-VCH, Weinheim, 1995.
5 M. R. J. Vos, G. E. Jardl, A. L. Pallas, M. Breurken, O. L. J. van Asselen, P. H. H. Bomans, P. E. L. G. Leclere, P. M. Frederik, R. J. M. Nolte and N. A. J. M. Sommerdijk, *J. Am. Chem. Soc.*, 2005, **127**, 16768–16769.
6 J. D. Tovar, R. C. Claussen and S. I. Stupp, *J. Am. Chem. Soc.*, 2005, **127**, 7337–7345.
7 M. Ambrosi, E. Fratini, V. Alfredsson, B. W. Ninham, R. Giorgi, P. Lo Nostro and P. Baglioni, *J. Am. Chem. Soc.*, 2006, **128**, 7209–7214.
8 P. Baglioni and D. Berti, *Curr. Opin. Colloid Interface Sci.*, 2003, **8**, 55–61.
9 D. Berti, *Curr. Opin. Colloid Interface Sci.*, 2006, **11**, 74–78.
10 M. Bonini, D. Berti, J. M. Di Meglio, M. Almgren, J. Teixeira and P. Baglioni, *Soft Matter*, 2005, **1**, 444–454.
11 J. Eastoe and A. Vesperinas, *Soft Matter*, 2005, **1**, 338–347.
12 H. Rosemeyer, *Chem. Biodiversity*, 2005, **2**, 977–1062.
13 C. Aime, S. Manet, T. Satoh, H. P. Ihara, F. K.-Y. Godde and R. Oda, *Langmuir*, 2007, ASAP.
14 S. E. Paramonov, H. W. Jun and J. D. Hartgerink, *J. Am. Chem. Soc.*, 2006, **128**, 7291–7298.
15 J. D. Hartgerink, E. Beniash and S. I. Stupp, *Science*, 2001, **294**, 1684–1688.
16 L. Moreau, P. Barthélémy, M. El Maataoui and M. W. Grinstaff, *J. Am. Chem. Soc.*, 2004, **126**, 7533.
17 X. Yan, H. Qiang, K. Wang, L. Duan, Y. Cui and L. Junbai, *Angew. Chem.*, 2007, **46**, 2431–2434.
18 M. B. H. Murphy, J.D., A. Goepferich and A. G Mikos, *Biomacromolecules*, 2007, **8**, 2237–2243.
19 V. M. H. Yuwono and J. D, *Langmuir*, 2007, **23**, 5033–5038.
20 D. Berti, P. L. Barbaro, I. Bucci and P. Baglioni, *J. Phys. Chem. B*, 1999, **103**, 4916–4922.
21 D. Berti, S. Bonaccio, G. Barsacchi-Bo, P. L. Luisi and P. Baglioni, *J. Phys. Chem. B*, 1998, **102**, 303–308.
22 D. Berti, L. Franchi, P. Baglioni and P. L. Luisi, *Langmuir*, 1997, **13**, 3438–3444.
23 F. Baldelli Bombelli, D. Berti, U. Keiderling and P. Baglioni, *J. Phys. Chem. B*, 2002, **106**, 11613–11621.
24 D. Berti, F. Baldelli Bombelli, M. Almgren and P. Baglioni, in *Self-Assembly*, ed. B. Robinson, IOS Press, Amsterdam, Editon edn, 2003.
25 F. Baldelli Bombelli, D. Berti, F. Pini, U. Keiderling and P. Baglioni, *J. Phys. Chem. B*, 2004, **108**, 16427–16434.

26 S. Shuto, S. Ueda, S. Imamura, K. Fukukawa, M. Tsujino, A. Matsuda and T. Ueda, *Chem. Pharm. Bull.*, 1988, **36**, 209.
27 D. Berti, P. L. Luisi and P. Baglioni, *Colloids Surf., A*, 2000, **167**, 95–103.
28 M. Banchelli, D. Berti and P. Baglioni, *Angew. Chem.*, 2007, **46**, 3070–3073.
29 S. Milani, F. Baldelli Bombelli, D. Berti and P. Baglioni, *J. Am. Chem. Soc.*, 2007, **129**, 11664–11665.
30 F. Baldelli Bombelli, D. Berti, U. Keiderling and P. Baglioni, *Appl. Phys. A*, 2002, **74**(Suppl.), S1270–S1273.
31 F. Baldelli Bombelli, D. Berti, M. Almgren, G. Karlsson and P. Baglioni, *J. Phys. Chem. B*, 2006, **110**, 17627–17637.
32 L. Cantu, M. Corti, E. Del Favero, E. Digirolamo and A. Raudino, *J. Phys. II*, 1996, **6**, 1067–1090.
33 P. Brocca, L. Cantu, M. Corti, E. Del Favero and A. Raudino, *Phys. A*, 2002, **304**, 177–190.
34 P. Brocca, L. Cantu, M. Corti, E. Del Favero and A. Raudino, *Langmuir*, 2007, **23**, 3067–3074.
35 S. U. Shuto, S. Imamura, K. Fukukawa, M. Tsujino, A. Matsuda and T. Ueda, *Chem. Pharm. Bull.*, 1988, **36**, 209.
36 M. Almgren, K. Edwards and G. Karlsson, *Colloids Surf., A*, 2000, **174**, 3–21.
37 S. W. Provencher, *Comput. Phys. Commun.*, 1982, **27**, 213.
38 U. Keiderling, *BerSANS Data reduction Manual*, HMI, Berlin, 1994.
39 M. Piotto, V. Saudek and V. J. Sklenar, *Biomol. NMR*, 1992, **2**, 661.
40 V. Sklenar, M. Piotto, R. Leppik and V. J. Saudek, *Magn. Res.*, 1993, **102**, 241.
41 J. Jeener, B. H. Meier, P. Bachmann and R. R. Ernst, *J. Chem. Phys.*, 1979, **71**, 4546.
42 V. Sklener, H. Miyashiro, G. Zon and H. T. Miles, *FEBS Lett.*, 1986, **208**, 94.
43 A. Bax and D. G. J. M. R. Davis, *J. Magn. Reson.*, 1985, **63**, 207.
44 A. A. Bothner-By, R. L. Stephens, J. M. Lee, C. D. Warren and R. W. J. A. C. S. Jeanloz, *J. Am. Chem. Soc.*, 1984, **106**, 811.
45 H. J. C. Berendsen, D. van der Spoel and R. van Drunen, *Comput. Phys. Commun.*, 1995, 91.
46 E. Lindahl, B. Hess and D. van der Spoel, *J. Mol. Model*, 2001, **7**, 306–317.
47 C. Oostenbrink, A. Villa, A. E. Mark and W. F. Van Gunsteren, *J. Comput. Chem.*, 2004, **25**, 1656–1676.
48 U. Essmann, L. Perera, M. L. Berkowitz, T. Darden, H. Lee and L. G. Pedersen, *J. Chem. Phys.*, 1995, **103**, 8577–8593.
49 B. Hess, H. Bekker, H. J. C. Berendsen and J. G. E. M. Fraaije, *J. Comput. Chem.*, 1997, **18**, 1463–1472.
50 W. Saenger, *Principles of Nucleic Acid Structure*, Springer-Verlag, New York, 1984.
51 P. Denkiger and W. Burchard, *J. Polym. Phys.*, 1991, **29**, 589.
52 A. Holtzer, *J. Polym. Sci.*, 1955, **17**, 432.
53 W. Saenger, *Angew. Chem., Int. Ed. Engl.*, 1973, **12**, 591–601.
54 W. Saenger, *Angew. Chem.*, 1973, **85**, 680–690.
55 W. Curtis Johnson Jr., Circular Dichroism and Its Empirical Application to Biopolymers, in *Methods of Biochemical Analysis*, ed. D. Glick, John Wiley & Sons, 1985, vol. 31, pp. 61–163.
56 W. Curtis Johnson, in *Circular Dichroism: Principles and Application*, ed. K. Nakanishi, N. Berova, R. J. Woody, VCH, New York, Editon edn, 1994, vol. 19, p. 523.
57 J. Brahms and W. H. F. M. Mommaerts, *J. Mol. Biol.*, 1964, **10**, 73–88.
58 J. M. Brahms, *J. Mol. Biol.*, 1965, **11**, 785–801.
59 J. M. Brahms, A.M. and K. E. Van Holde, *J. Mol. Biol.*, 1966, **15**, 467–488.
60 J. M. Brahms, J.C. and A. M. Michelson, *J. Mol. Biol.*, 1967, **25**, 481–495.
61 D. W. Miles, L. B. Townsend, P. Redington and H. Eyring, *Proc. Natl. Acad. Sci. U. S. A.*, 1976, **73**, 2384–2387.
62 D. W. Miles, L. B. Townsend, D. L. Miles and H. Eyring, *Proc. Natl. Acad. Sci. U. S. A.*, 1978, **76**, 553–556.
63 V. A. Bloomfield, D. M. Crothers and I. Tinoco, *Nucleic Acids. Structures, Properties and Functions*, University Science Books, Sausalito, California, 2000.
64 D. B. Davies, *Prog. Nucl. Magn. Reson. Spectrosc.*, 1978, **12**, 135.
65 P. A. Hart and J. P. Davis, *J. Am. Chem. Soc.*, 1973, **93**, 753–760.
66 H. Dugas, B. J. Balckburn, R. K. Robins, R. Deslauriers and I. C. P. Smith, *J. Am. Chem. Soc.*, 1973, **93**, 3468–3470.
67 M. P. Schweizer, J. T. Witkowski and R. K. Robins, *J. Am. Chem. Soc.*, 1971, **93**, 277–279.
68 D. W. Miles, L. B. Townsend, D. L. Miles and H. Eyring, *Proc. Natl. Acad. Sci. U. S. A.*, 1973, **76**, 553–556.
69 M. P. Schweizer, E. B. Banta, J. T. Witkowski and R. K. Robins, *J. Am. Chem. Soc.*, 1973, **95**, 3770–3778.
70 T. Bandyopadhyay, J. Wu, W. A. Stripe, I. Carmichael and A. S. Serianni, *J. Am. Chem. Soc.*, 1997, **119**, 1737.
71 S. T. Rao and M. Sundaralingam, *J. Am. Chem. Soc.*, 1976, **92**, 4963–4970.
72 D. Suck and W. Saenger, *J. Am. Chem. Soc.*, 1972, **94**, 6520–6526.
73 R. K. Nanda, R. Tewari, G. Govil and I. C. P. Smith, *Can. J. Chem.*, 1974, **52**, 371–375.
74 A. L. George, F. E. Hruska, K. K. Ogilvie and A. Holy, *Can. J. Chem.*, 1974, **56**, 1170–1176.
75 J. Kallen, C. Spitzfaden, M. G. M. Zurini, G. Wider, H. Widmer, K. Wüthrich and M. D. Walkinshaw, *Nature*, 1991, **353**, 276.
76 (*a*) A. Bax and L. Lerner, *Science*, 1986, 960; (*b*) A. Kumar, G. Wagner, R. R. Ernst and K. Wüthrich, *J. Am. Chem. Soc.*, 1981, **103**, 3654; (*c*) I. Goljer and P. H. Bolton, in *Two-Dimensional NMR Spectroscopy, Application for Chemists and Biochemists*, ed., W. R. Croasmun and R. M. K. Carlson, VCH, New York, 2nd edn, 1994; (*d*) C. Griesinger and R. R. J. Ernst, *Magn. Reson.*, 1987, **75**, 261; (*e*) D. Neuhaus and J. J. Keeler, *Magn. Reson.*, 1986, **68**, 568; (*f*) D. Neuhaus; M. Williamson, *The Nuclear Overhauser Effect in Structural and Conformational Analysis*, VCH, New York, 1989; (*g*) W. Braun, C. Bösch, L. R. Brown, N. Go and K. Wüthrich, *Biochim. Biophys. Acta*, 1981, **667**, 377; (*h*) K. Wüthrich, *Acc. Chem. Res.*, 1989, **22**, 36.
77 (*a*) J. H. Noggle and R. E. Schirmer, *The Nuclear Overhauser Effect*, Academic Press, New York, 1971; (*b*) J. Jeener, B. H. Meier, P. Bachmann and R. R. J. Ernst, *Chem. Phys.*, 1979, **71**, 4546; (*c*) S. Macura, K. Wüthrich and R. R. J. Ernst, *Magn. Reson.*, 1982, **47**, 351.
78 (*a*) H. Rosemeyer, G. G. Tóth, B., Z. Kazimierczuk, W. Bourgeois, U. Kretschmer, H. P. Muth and F. Seela, *J. Org. Chem.*, 1990, **55**, 5784; (*b*) M. Polak, K. L. Seley and J. Plavec, *J. Am. Chem. Soc.*, 2004, **126**, 8159.
79 (*a*) S. L. Gordon and K. Wüthrich, *J. Am. Chem. Soc.*, 1978, 7094; (*b*) S. Macura and R. R. Ernst, *Mol. Phys.*, 1980, **41**, 95.
80 R. R. Ernst, G. Bodenhause and A. Wokaun, *Principles of Nuclear Magnetic Resonance in One and Two Dimensions*, Oxford University Press, Oxford, 1987.
81 L. D. Field, M. G. Gardiner, B. A. Messerle and C. L. Raston, *Organometallics*, 1992, **11**, 3566.
82 N. Foloppe and L. Nilsson, *J. Phys. Chem. B*, 2005, **109**, 9119–9131.
83 A. D. MacKerell and N. K. Banavali, *J. Comput. Chem.*, 2000, **21**, 105–120.
84 R. Soliva, F. J. Luque, C. Alhambra and M. Orozco, *J. Biomol. Struct. Dyn.*, 1999, **17**, 89–99.
85 S. T. Rao, E. Westhof and M. Sundaralingam, *Acta Crystallogr., Sect. A: Cryst. Phys., Diffr., Theor. Gen. Cryst.*, 1981, **37**, 421–425.
86 S. Shibata, *Magn. Reson. Chem.*, 1992, **30**, 371–376.
87 W. Humphrey, A. Dalke and K. Schulten, *J. Mol. Graphics*, 1996, **14**, 33-&.
88 M. Banyay, M. Sarkar and A. Graslund, *Biophys. Chem.*, 2003, **104**, 477–488.
89 S. Adam, P. Bourtayre, J. Liquier and E. Taillandier, *Nucleic Acids Res.*, 1986, **14**, 35013513.
90 M. Ghomi, J. A. Taboury and E. Taillandier, *Biochemie*, 1984, **66**, 87–92.
91 J. Liquier and E. Taillanddier, in *Infrared spectroscopy of Biomolecules*, ed. D. Chapman, Wiley-Liss Inc., New York, Editon edn, 1996, pp. 131–158.
92 U. P. Fringeli and H. H. Gunthard, in *Membrane Spectrosocpy*, ed. E. Grell, Springer-Verlag, Berlin, Editon edn., 1981.
93 L. Senak, M. A. Davies and R. Mendelsoh, *J. Phys. Chem.*, 1991, **95**, 2565–2571.
94 H. L. Casal and R. N. McElhaney, *Biochemistry*, 1990, **29**, 5423–5427.
95 V. J. Selinger, M. S. Spector and J. M. Schnur, *J. Phys. Chem. B*, 2001, **105**, 7158–7169.
96 T. Shimizu, M. Mitsutoshi and H. Minamikawa, *Chem. Rev.*, 2005, **105**, 1401–1443.
97 A. Brizard, C. Aime, T. Labrot, I. Huc, D. Berthier, F. Artzner, B. Desbat and R. Oda, *J. Am. Chem. Soc.*, 2007, **129**, 3754–3762.